New Journal of Physics
The open access journal at the forefront of physics

Deutsche Physikalische Gesellschaft DPG
IOP Institute of Physics

Published in partnership with: Deutsche Physikalische Gesellschaft and the Institute of Physics

OPEN ACCESS

RECEIVED
30 November 2020

REVISED
5 February 2021

ACCEPTED FOR PUBLICATION
8 February 2021

PUBLISHED
9 March 2021

PAPER

Optical simulation of quantum mechanics on the Möbius strip, Klein's bottle and other manifolds, and Talbot effect

J Bělín[1,2,*], T Tyc[3] and S A R Horsley[4]

[1] School of Physics and Astronomy, College of Science and Engineering, University of Glasgow, Glasgow G12 8QQ, United Kingdom
[2] Central European Institute of Technology, Brno University of Technology, Purkyňova 656/123, 612 00 Brno, Czech Republic
[3] Department of Theoretical Physics and Astrophysics, Faculty of Science, Masaryk University, Kotlářská 2, 61137 Brno, Czech Republic
[4] Department of Physics and Astronomy, Stocker Road, University of Exeter, Exeter EX4 4QL, United Kingdom
[*] Author to whom any correspondence should be addressed.

E-mail: Jakub.Belin@ceitec.vutbr.cz, tomtyc@physics.muni.cz and S.Horsley@exeter.ac.uk

Keywords: curved spaces, quantum revivals, Talbot effect, topology, orbifolds

Abstract

We analyse the evolution of the wavefunction of a quantum particle propagating on several compact manifolds, including the Klein bottle, Möbius strip and projective plane. We find analytically the stationary states and the energy spectrum and show that the wavefunction exhibits perfect revivals. Using the orbifold structure of the discussed manifolds, we establish the relation of wave evolution on the manifolds to Fresnel diffraction and consequently to the Talbot effect. This connection provides a novel method of optical simulation of the quantum motion on compact manifolds. We discuss some novel phenomena as well as the effects of topology on the properties of the waves on the manifolds.

1. Introduction

Wave propagation on a closed surface differs markedly from that on an open one. Rather than escape to infinity the wave energy continually revisits parts of the surface, allowing the formation of bound states. The local curvature of the surface also affects the wave: positive Gaussian curvature tends to focus wave energy, and negative curvature tends to disperse it [1]. One can therefore control a wave that is confined to a surface through carefully shaping the surface, which is the principle of geodesic lens design [2–5]. Indeed, the control of a wave through modifying the local geometry goes deeper than this, and transformation optics [6–8] has recently exploited the equivalence between material parameters and geometry to design concealment devices [9–11], among other things. This work is in a similar vein, but rather than focus on controlling propagation through changing the local geometry seen by the wave, we change the *topology* of the space. Topology is concerned with global properties of the geometry, and is well known to affect the behaviour of a wave confined to a surface. For instance, the Poincare–Hopf theorem [12] tells us that any standing wave on a closed surface will have critical points related to the Euler characteristic of the surface.

Here we consider a number of manifolds with different topologies and Euler characteristics: a torus, Möbius strip, Klein bottle, real projective plane, 'double-sided square' [13], and 'double-sided triangle'. Extending the previous work of reference [14] where some of these manifolds were also considered, we establish an equivalence of wave propagation on the manifolds with wave propagation on their quotient spaces, equipped with the appropriate boundary conditions ('gluing instructions'). Arranging copies of the quotient space in a plane without gaps and overlaps such that the gluing instructions are satisfied at boundaries between adjacent copies, we find that this equivalence can be further extended to wave propagation in the plane, subject to the symmetries derived from the symmetry and topology of the original manifold. This enables us to find analytically the modes and eigenfrequencies for the manifolds. Remarkably, thanks to the spectrum structure, each of the manifolds considered here exhibits perfect wavefunction revivals.

Moreover, thanks to the equivalence between paraxial wave propagation along an axis and time evolution according to the time dependent Schrödinger equation, we show that the time evolution of a Schrödinger wave on the manifold is equivalent to the evolution of the diffraction pattern created by a grating of a particular symmetry. This enables an efficient optical simulation of quantum wave propagation on the manifolds: simply illuminate a grating with the particular symmetry by a plane wave and observe the diffraction patterns at different distances behind it. The wavefunction revivals then correspond to the Talbot effect for the corresponding diffraction problem.

Thanks to the periodicity of the wave in the plane tessellated by the copies of the quotient space, the evolution of the quantum wave on any of the manifolds considered here is always equivalent to evolution of a quantum wave on the surface of some torus, usually larger than the quotient space. However, for most of the manifolds considered here (all but the torus itself) there is a smaller repeat pattern which satisfies boundary conditions equivalent to folds or twists in the surface, and therefore the wave behaves as if on a closed surface with a different topology than that of the torus. This fact is already well known to mathematicians, and forms the basis of Conway's orbifold description of the wallpaper group [15].

The paper is organised as follows: in sections 2 and 3 we discuss the quotient space of a manifold and its tessellation of a plane, respectively. In section 4 we describe the method for finding the modes analytically and present eigenmodes and eigenvalues for different manifolds. In section 5 we establish the relation with paraxial diffraction theory. In section 6 we present numerical simulations of wavepacket evolution, including demonstration of topological charge reversal on the Klein bottle. In section 7 we discuss the relation of the manifold topology to the properties of the critical points of its modes, and we conclude in section 8.

2. Manifold and its quotient space

Consider a quantum particle of mass μ propagating freely (i.e., in zero potential) on a closed manifold S. The Hamiltonian is then $\hat{H} = -\frac{\hbar^2}{2\mu}\triangle$, where $\triangle$ is the Laplacian. The Schrödinger equation

$$\mathrm{i}\hbar\frac{\partial\psi}{\partial t} = \hat{H}\psi = -\frac{\hbar^2}{2\mu}\triangle\psi \tag{1}$$

has separable solutions of the form $\psi_n(\vec{r},t) = \psi_n(\vec{r})\exp(-\mathrm{i}E_n t/\hbar)$, where the stationary states $\psi_n(\vec{r})$ satisfy the Helmholtz equation

$$\triangle\psi_n + k_n^2\psi_n = 0, \tag{2}$$

where k_n is the wavenumber and the energy eigenvalues are $E_n = \hbar^2 k_n^2/(2\mu)$.

Instead of solving the Helmholtz equation on the manifold itself, we can equivalently solve it on the *quotient space*, i.e., on the unfolded net of the manifold equipped with 'gluing instructions'—the rules of which edges of the unfolded net should be identified. This key observation has been made in reference [16] and was further exploited in reference [17] for the case of a regular tetrahedron where the quotient space is an equilateral triangle. This does not solve the problem completely, and finding the modes for many quotient spaces is still difficult. However, the problem is greatly simplified if copies of the quotient space can be arranged such that they fill the entire Euclidean plane, without gaps or overlaps, such that the gluing instructions are satisfied even at the boundaries between different copies of the quotient space. In that case one can solve the Helmholtz equation in the plane directly instead of the quotient space; the only restriction is that the wavefunction has to have the same values on all the copies of the quotient space. This imposes certain restrictions on the wavefunction periodicity and/or other types of symmetry, and leads to discrete modes. In the case of tetrahedron, these modes are standing plane waves. In the following we will analyse a number of other manifolds whose quotient spaces can tessellate the plane, and find their modes.

3. Tessellating the plane with quotient space

In this section we establish the relation between waves on a manifold whose quotient space can tessellate the plane, and the waves in that plane. This will then be further used for finding modes on the manifold.

Consider a manifold S which can be unfolded to a quotient space σ with a set gluing instructions such that the entire plane $\mathbb{R}^2$ can be tessellated with copies of σ, without any overlaps or gaps, and with the gluing instructions satisfied in $\mathbb{R}^2$, i.e., the identified edges of different copies of σ are connected with the correct orientation. Such surface has an orbifold structure [15].

Further, consider a function $\psi_0(x,y)$ defined on the quotient space σ that satisfies the Helmholtz equation (2) with wavenumber k as well as the gluing instructions. This function represents a *mode* on the

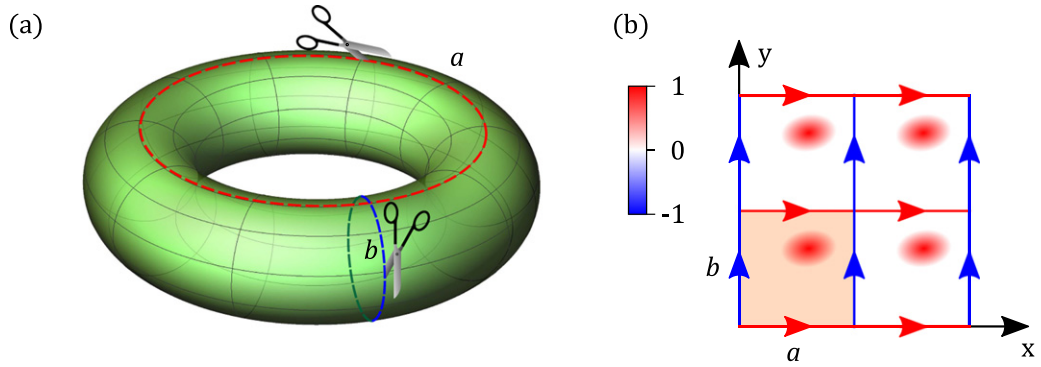

Figure 1. (a) A torus and (b) its quotient space σ along with the tessellation of the plane $\mathbb{R}^2$ by copies of σ. The quotient space is a rectangle of sides a and b marked by the orange shading with its opposite sides identified by relations $(0, y) \sim (a, y)$ and $(x, 0) \sim (x, b)$, which is indicated with red and blue arrows. The red spots represent a sample Gaussian wavefunction and help to visualise the tessellation.

manifold. We would now like to define the equivalent mode $\psi(x, y)$ on the whole plane $\mathbb{R}^2$, generated from $\psi_0(x, y)$ by the tessellation of $\mathbb{R}^2$ with copies of the quotient space. Similar as $\psi_0(x, y)$, we require also $\psi(x, y)$ to satisfy the Helmholtz equation, this time in the whole plane.

In the following we have to distinguish two classes of manifolds and treat them separately: the first class contains manifolds without hard boundaries, i.e., without lines on which the wavefunction has to vanish. These include surfaces of polyhedra, the torus, the Klein's bottle etc. The second class are manifolds with hard boundaries on which the wavefunction has to be zero. These include polygons with hard walls, the Möbius strip etc.

3.1. Manifolds without hard boundaries

For the first class of manifolds, namely those that contain no hard boundaries, going from the function $\psi_0(x, y)$ on the quotient space to the equivalent function $\psi(x, y)$ in the plane is straightforward: the function $\psi(x, y)$ is simply equal to $\psi_0(x, y)$ for the respective copy of the quotient space. This is illustrated in figure 1(b) for the case of a torus whose quotient space is a rectangle with sides a and b, and the pairs of opposite sides are identified. The tiling is performed simply by attaching the individual copies of σ to each other with the same orientation, forming a periodic rectangular structure with periods a and b in the x and y directions, respectively. The function $\psi(x, y)$ is then also periodic, with the same periods.

3.2. Manifolds with hard boundaries

For the second class of manifolds, namely those that do contain hard boundaries, we have to deal with these boundaries carefully. Let l be one of the straight lines that form the hard boundary in the quotient space σ; this means that the function $\psi_0(x, y)$ is identically zero on l. We will call l a 'zero line'. We would now like to achieve the same condition for the equivalent function $\psi(x, y)$ in the plane $\mathbb{R}^2$ that is tiled with copies of σ, but at the same time we require $\psi(x, y)$ to be the solution of the Helmholtz equation in the whole plane (which also means that it is continuous including its first derivatives). A natural way how to combine these requirements is as follows: to the zero line l on a given tile (i.e., on a copy on σ) we attach another tile again with the corresponding zero line l such that the copies of σ meeting at l are mirror images of each other with respect to l. Moreover, one of these two tiles will be taken as 'negative', meaning that the function $\psi(x, y)$ on that tile is equal to $-\psi_0(x, y)$ on σ; the other tile is 'positive' and the function $\psi(x, y)$ on it is simply equal to $\psi_0(x, y)$ on σ. This ensures that the derivative of $\psi(x, y)$ normal to l is continuous when going from one tile to the other. We illustrate this on an example of the Möbius strip with dimensions a and b, depicted in figure 2. The function $\psi(x, y)$ in the plane $\mathbb{R}^2$ has periodicity $2a$ and $2b$, respectively, because of alternating positive and negative tiles.

4. Mode structure of the manifold

By establishing equivalence of Helmholtz equation solutions $\psi_0(x, y)$ on the quotient space σ with the solutions $\psi(x, y)$ in the plane $\mathbb{R}^2$ we have obtained a powerful tool for finding the modes. Indeed, since the tessellation of the plane $\mathbb{R}^2$ with copies of the quotient space σ according to the above rules is periodic, the

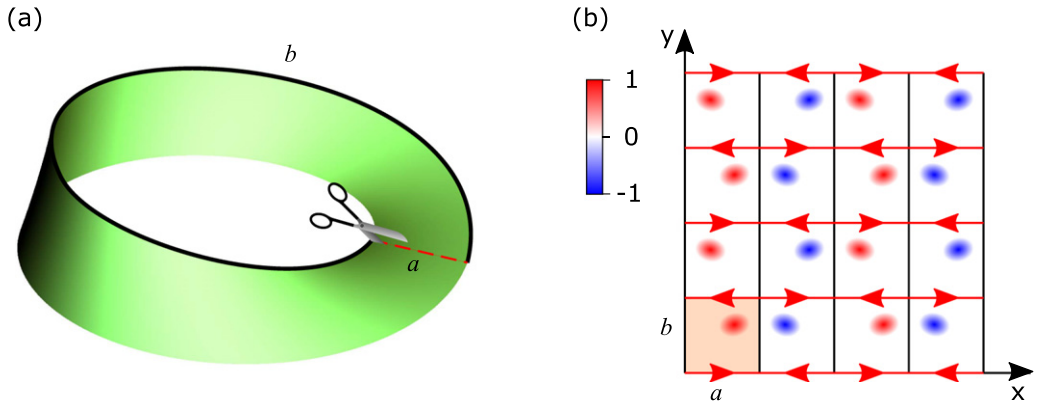

Figure 2. (a) Möbius strip and (b) the corresponding quotient space σ (again marked by the orange shading) and its tessellation of the plane. The tiles with blue spots are negative in the sense described in the text, and the wavefunction is zero on the black lines.

resulting function $\psi(x, y)$ is periodic as well. If we introduce its Fourier transform,

$$\tilde{\psi}(k_x, k_y) = \frac{1}{2\pi} \int_{\mathbb{R}^2} \psi(x, y) \mathrm{e}^{-\mathrm{i}(k_x x + k_y y)} \, \mathrm{d}x \, \mathrm{d}y, \tag{3}$$

the periodicity of $\psi(x, y)$ implies that the function $\tilde{\psi}(k_x, k_y)$ is nonzero only on a discrete comb of points in the plane (k_x, k_y) (i.e., in the reciprocal space). Moreover, from the fact that the function $\psi(x, y)$ is a solution of the Helmholtz equation in the plane $\mathbb{R}^2$ (with the wavenumber k) then follows that $\tilde{\psi}(k_x, k_y)$ is nonzero only on the circle $k_x^2 + k_y^2 = k^2$. Combining these two restrictions on the function $\tilde{\psi}(k_x, k_y)$, we arrive at the fact that this function is nonzero only on a finite number of discrete points in the reciprocal space, which means that each of the modes we are looking for is a superposition of a finite number of plane waves. The form of this superposition depends on the manifold we are dealing with; we will show that it can be deduced from the symmetries of the tessellation of the plane with copies of σ.

For example, consider a sample Gaussian function $\psi_0(x, y)$ defined on the quotient space σ of the Möbius strip and depicted in the bottom-left orange-shaded square in figure 2(b). Tessellation of the plane with copies of σ results in the function $\psi(x, y)$ as explained in section 3, depicted in the entire panel figure 2(b). One can see that the function $\psi(x, y)$ has a translational symmetry $\psi(x, y) = \psi(x + 2ma, y) = \psi(x, y + 2nb)$, where $m, n \in \mathbb{Z}$. This symmetry then implies the allowed values of the components k_x, k_y of the wavevector $\mathbf{k} = (k_x, k_y)$, i.e. $k_x = m\pi/a$ and $k_y = n\pi/b$. Additionally, the following symmetries of function $\psi(x, y)$ can be deduced from figure 2(b): $\psi(x, y) = -\psi(-x, y)$, $\psi(x, y) = -\psi(x + a, y + b)$, $\psi(x, y) = \psi(-x + a, y + b)$. The function satisfying these symmetries is an eigenmode of the Möbius strip and can be represented as the following superposition of plane waves

$$\begin{aligned} \psi_{mn}(x, y) = \frac{N_{mn}}{4\mathrm{i}} \Bigg[& \exp \mathrm{i}\pi \left(\frac{mx}{a} + \frac{ny}{b} \right) - \exp \mathrm{i}\pi \left(-\frac{mx}{a} + \frac{ny}{b} \right) \\ & - \exp \mathrm{i}\pi \left(\frac{m(x + a)}{a} + \frac{n(y + b)}{b} \right) + \exp \mathrm{i}\pi \left(\frac{m(-x + a)}{a} + \frac{n(y + b)}{b} \right) \Bigg] \\ = & \sqrt{\frac{2}{ab}} \sin \left(\frac{m\pi x}{a} \right) \exp \left(\frac{\mathrm{i}\pi n y}{b} \right), \end{aligned} \tag{4}$$

where $N_{mn} = (2/ab)^{1/2}$ is a normalizing constant, $m \in \mathbb{N}, n \in \mathbb{Z}$, and the number $m + n$ must be odd. The same result may be obtained by applying the boundary conditions of the quotient space σ directly.

Applying the symmetries of the tessellation of the plane with copies of the quotient space σ, one can find the modes of some other manifolds, including torus, Klein bottle, real projective plane, double-sided square and the double-sided triangle (we will provide the definitions of the last two manifolds in the appendices A and B). Klein bottle and the real projective plane, together with the tessellation of plane $\mathbb{R}^2$ with copies of their respective quotient spaces, are presented in figure 3. Modes of all the manifolds mentioned above, together with their normalizing constants, are presented in table 1.

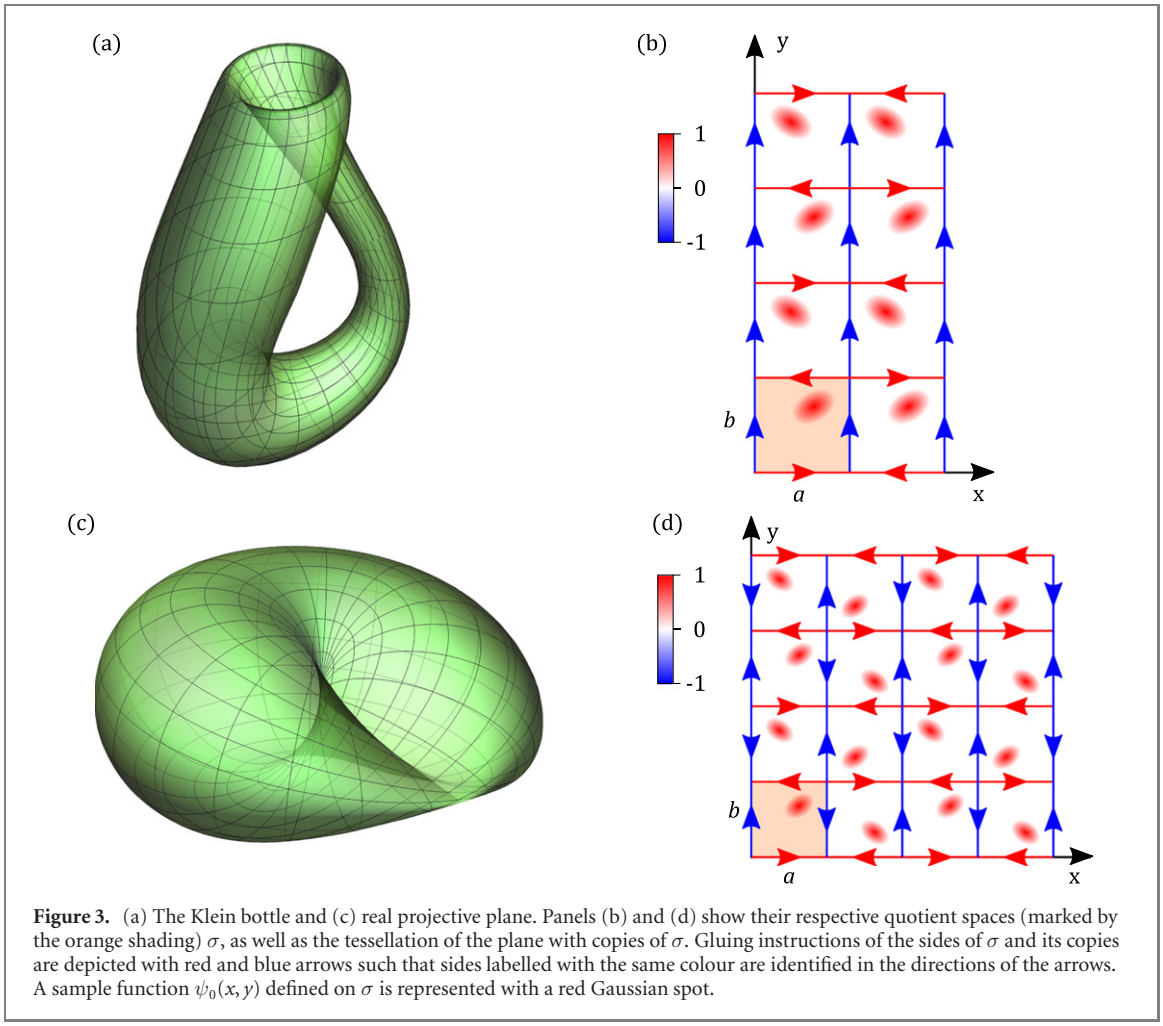

Figure 3. (a) The Klein bottle and (c) real projective plane. Panels (b) and (d) show their respective quotient spaces (marked by the orange shading) σ, as well as the tessellation of the plane with copies of σ. Gluing instructions of the sides of σ and its copies are depicted with red and blue arrows such that sides labelled with the same colour are identified in the directions of the arrows. A sample function $\psi_0(x, y)$ defined on σ is represented with a red Gaussian spot.

Table 1. Modes of closed manifolds, obtained by investigating the symmetries of the tessellation of the plane with copies of the respective quotient space σ.

Surface	Mode ψ_{mn}
Torus	$(ab)^{-\frac{1}{2}} \exp\left[2\pi \mathrm{i}\left(\frac{mx}{a}+\frac{ny}{b}\right)\right]$
Klein bottle	$\left[ab(1+\delta_{0m})/2\right]^{-\frac{1}{2}} \cos\left[\pi\left(\frac{2mx}{a}-\frac{n}{2}\right)\right] \exp\left(\frac{\mathrm{i}\pi ny}{b}\right)$
Real projective plane	$\left[ab\,(1+\delta_{m0})\,(1+\delta_{n0})\,/4\right]^{-\frac{1}{2}} \cos\left[\pi\left(\frac{mx}{a}+\frac{m+n}{2}\right)\right] \cos\left[\pi\left(\frac{ny}{b}+\frac{m+n}{2}\right)\right]$
Double-sided square	$a^{-1}[(1+\delta_{m0}\delta_{n0})/2]^{-\frac{1}{2}} \cos\left\{\frac{\pi}{a}\left[(m+n)x+(m-n)\left(y-\frac{a}{2}\right)\right]\right\}$
Double-sided triangle	$\left(3\sqrt{3}a^2(1+2\delta_{m0}\delta_{n0})/2\right)^{-\frac{1}{2}} \left\{\exp\left[\frac{\mathrm{i}\pi}{a}\left(\frac{2m}{3}x+\frac{2n}{\sqrt{3}}y\right)\right]+\exp\left[\frac{\mathrm{i}\pi}{a}\left(\frac{-m+3n}{3}x-\frac{m+n}{\sqrt{3}}y\right)\right]\right.$ $\left.+\exp\left[\frac{\mathrm{i}\pi}{a}\left(-\frac{m+3n}{3}x+\frac{m-n}{\sqrt{3}}y\right)\right]\right\}$

5. Connection to the diffraction theory

In this section, we will show how the quantum motion on compact manifolds is related to Fresnel diffraction on periodic lattices and, consequently, to the Talbot effect. It is a well known fact that paraxial propagation of a monochromatic scalar wave in a 3D space along the z axis is equivalent to time evolution of a free quantum particle in a 2D plane [18]. Indeed, the paraxial Helmholtz equation in free space can be written as

$$\mathrm{i}k_0 \frac{\partial \psi}{\partial z} = -\frac{1}{2}\triangle_{\mathrm{T}}\psi, \tag{5}$$

where $\triangle_{\mathrm{T}} = \partial^2/\partial x^2 + \partial^2/\partial y^2$ is the 2D Laplace operator, k_0 is the wavenumber of the wave, and the global phase factor $\exp(\mathrm{i}k_0 z)$ of the wave ψ has been omitted. Equation (5) is equivalent to the Schrödinger equation (1) if we set $z = \hbar k_0 t/\mu$. This equivalence leads to an interesting way of optically simulating (or visualising) evolution of a free quantum particle in a plane: one can simply perform a paraxial diffraction

Table 2. Energy spectra and revival times T of chosen closed manifolds.

Surface	Energy spectrum E_{mn}	Revival time T for $a = b$
Torus	$2\pi^2\hbar^2(m^2/a^2 + n^2/b^2)/\mu$	$\mu a^2/(\pi\hbar)$
Möbius strip	$\pi^2\hbar^2(m^2/a^2 + n^2/b^2)/(2\mu)$	$4\mu a^2/(\pi\hbar)$
Klein bottle	$\pi^2\hbar^2(4m^2/a^2 + n^2/b^2)/(2\mu)$	$4\mu a^2/(\pi\hbar)$
Real projective plane	$\pi^2\hbar^2(m^2/a^2 + n^2/b^2)/(2\mu)$	$4\mu a^2/(\pi\hbar)$
Double-sided square	$\pi^2\hbar^2(m^2 + n^2)/(\mu a^2)$	$2\mu a^2/(\pi\hbar)$
Double-sided triangle	$2\pi^2\hbar^2(m^2 + 3n^2)/(9\mu a^2)$	$9\mu a^2/(4\pi\hbar)$

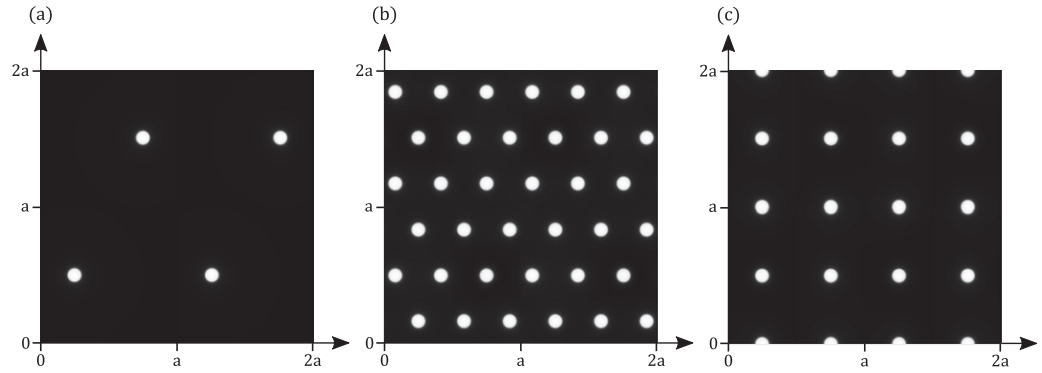

Figure 4. Evolution of the state (represented by the probability density) on the Klein bottle shown at (a) $t = 0$ (initial state), (b) $t = T/6$ and (c) $t = T/8$. Note that in (b) the probability density exhibits an almost hexagonal symmetry while in (c) its symmetry is rectangular.

experiment, letting a collimated beam incident on a grating placed in the plane $z = 0$ whose complex transmission function corresponds to the initial state of the quantum particle; the evolution of the light wave along the z axis then corresponds to the time evolution of the quantum particle.

On the other hand, we have seen that for a manifold S whose quotient space σ can tessellate the entire plane $\mathbb{R}^2$ with the corresponding gluing instructions, propagation of a quantum particle on S is equivalent to its propagation in the plane $\mathbb{R}^2$. Combining this idea with the above observation, we arrive at an interesting conclusion: evolution of a quantum particle on the manifold S is equivalent to diffraction on a grating whose complex transmission function satisfies the gluing instructions induced by the tessellation of the plane by the copies of the quotient space σ (in other words, the grating has to obey the symmetry of the tessellation). This enables to simulate the quantum motion on closed surfaces with simple diffraction experiments. Moreover, if the quantum particle exhibits perfect quantum state revivals with the revival time T, in the diffraction problem we will observe the Talbot effect [19–23] with the Talbot distance $z_T = \hbar k_0 T/\mu$. This is a generalisation of similar observations made previously for the case of the tetrahedron [17]. For each manifold presented in this paper, we have calculated the eigenvalues E_{mn} of the Hamiltonian $\hat{H} = -\frac{\hbar^2}{2\mu}\triangle$. For a special choice $a = b$ of the dimensions of the respective quotient space, we also calculated the revival time T. Both energy spectra E_{mn} and revival times T are presented in table 2.

6. Simulations

In this section we present numerical simulations of quantum motion on some of the manifolds discussed above. Wherever the quotient space was a rectangle with sides a and b, we have made it square by setting $a = b$. All the figures show a section of the plane containing several copies of the quotient space. The plots show the magnitude of the wavefunction $\psi(x, y, t)$ (expressed as brightness) at different rational multiples of the revival time T. The simulations were performed using Matlab and Mathematica.

Figure 4 visualises quantum motion of a particle on the Klein bottle. The initial state is chosen to be constant on a disk and zero elsewhere. We can observe an interesting phenomenon: whereas the probability density at time $T/8$ has a rectangular symmetry, the pattern at time $T/6$ exhibits an almost hexagonal symmetry. This is caused by the arrangements of the fractional Talbot images at the corresponding times. Figure 5 visualises quantum motion of a particle on the Möbius strip with a similar initial state as for the Klein bottle, just using a larger disk.

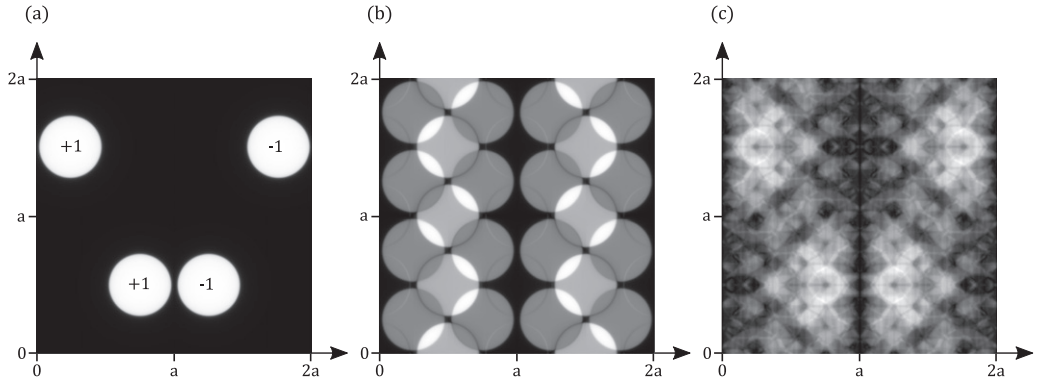

Figure 5. Evolution of the state on the Möbius strip shown at (a) $t = 0$ (initial state), (b) $t = T/4$ and (c) $t = 2T/13$. In (a) the signs of the initial wavefunction at different copies of the quotient space are marked.

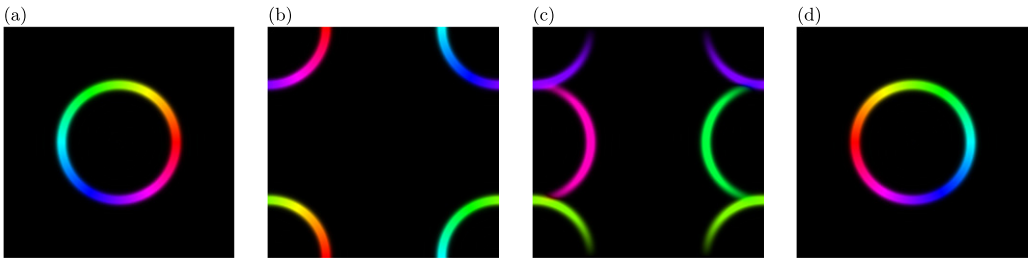

Figure 6. Wave evolution on the torus and Klein bottle; the brightness encodes the wave amplitude while the hue encodes the phase. Panel (a) shows the identical initial state on both manifolds at time $t = 0$, having the topological charge of $+1$. Panels (b) and (c) show the state at time $t = \mu a^2/(2\pi\hbar)$ on the torus and the Klein bottle, respectively. Panel (d) shows the state on the Klein bottle at time $t = 2\mu a^2/(\pi\hbar)$. Note that the topological charge has reversed to -1 due to the non-orientable nature of the Klein bottle. The wavefunction of the torus at this time returns to the initial state of (a) because it is twice the revival time of the torus.

Figure 6 compares quantum motion of a particle on the torus and the Klein bottle. The initial state was chosen to have a topological charge of $+1$. Remarkably, on the Klein bottle the wave evolves such that it has a topological charge of -1 at half of the Talbot time [see figure 6(d)]. This topological charge flip never happens for the torus and it is caused by the non-orientability of the Klein bottle. This way, we see that there appears a new wave phenomenon due to the different topology of the Klein bottle.

7. The effect of topology on the critical points of the modes

As mentioned in the Introduction, topology has an effect on the allowed waves in a space. We now show that this is evident in the modes given in the previous sections. All of our closed manifolds can be classified in terms of their Euler characteristic $\chi = 2(1 - g)$, where g is the number of holes in the surface. Table 3 shows the Euler characteristics of the closed surfaces considered above in section 6. Famously the Euler characteristic appears in the Gauss–Bonnet theorem [24], where it equals the integrated surface curvature divided by 2π. The Euler characteristic also governs the behaviour of a vector field $\boldsymbol{v}$ on a closed surface. In particular it specifies how the vector should behave at its isolated critical points $\boldsymbol{x}_n$, these being where the vector has an undefined direction (we do not consider vector fields with non-isolated critical points). The Poincare–Hopf theorem [12] states that

$$\sum_n \mathrm{index}_{\boldsymbol{x}_n}(\boldsymbol{v}) = \chi. \tag{6}$$

The 'index' of the vector field $\boldsymbol{v}$ at each of the critical points is the winding of the vector around the point. It is calculated by taking an anticlockwise path around the critical point and recording how many times the vector rotates as we move around the loop: n anticlockwise rotations of $\boldsymbol{v}$ corresponds to an index of $+n$, and an index of $-n$ corresponds to n clockwise rotations. As a simple example of a vector with a critical point, take the radius vector $\boldsymbol{r} = (x, y)$. The radius vector has a critical point at the origin, where its direction is undefined, and as we move in a small circle enclosing the origin the vector makes one anticlockwise rotation, hence it is a critical point with index $+1$.

Table 3. Euler characteristics for closed manifolds without boundaries given in section 6.

Surface	Euler characteristic χ
Torus	0
Klein bottle	0
Real projective plane	1
Double-sided square	2
Double-sided triangle	2

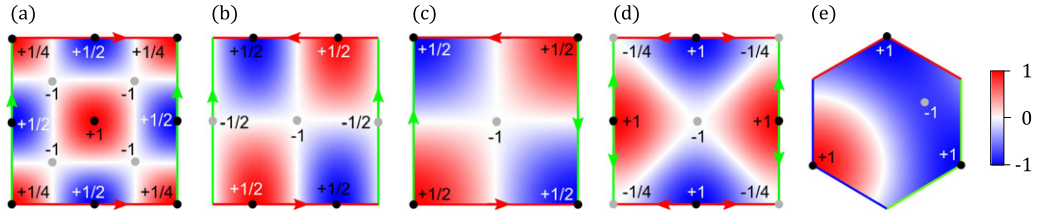

Figure 7. (a) Torus with the mode $\psi = \psi_{1,1} + \psi_{-1,1} + \psi_{1,-1} + \psi_{-1,-1}$. (b) Klein bottle with the mode $\psi = \psi_{1,1} + \psi_{1,-1}$. (c) Real projective plane with $\psi = \psi_{1,1}$. (d) Double-sided square with $\psi = \psi_{1,1} + \psi_{1,-1}$. (d) Double-sided triangle with $\psi = \psi_{1,1} + \psi_{-1,-1}$. Maxima/minima are labelled with black dots, whereas saddle points are marked with grey dots. Since some critical points are identified according to the gluing instructions (e.g. all the black dots in the corners of the torus quotient space in (a) actually correspond to a single point), we have to multiply their indexes with the factors 1/2 or 1/4, which gives the numbers shown.

This theorem can be applied to the modes on the closed manifolds investigated in the previous sections. For the manifolds with boundaries there is an additional boundary contribution to (6), a complication which we do not consider here. To see that the modes of the closed manifolds really satisfy the theorem, we have constructed for each manifold a real-valued superposition of the simplest degenerate modes $\psi = \sum_{mn} c_{mn}\psi_{mn}$, with isolated maxima, minima, and saddle points, see figure 7. The gradient of each such mode $\boldsymbol{v} = \boldsymbol{\nabla}\psi$ is a vector field to which the theorem (6) applies. At every maximum or minimum of ψ, $\boldsymbol{v}$ has an index of $+1$, while at saddle points of the mode $\boldsymbol{v}$ will have an index of -1. Counting in figure 7 the contributions of the maxima, minima, and saddle points, we arrive at the correct Euler characteristics according to table 3, which shows that the modes indeed reflect the topology of our different manifolds.

8. Conclusions

We have found analytically eigenfunctions and eigenvalues for the stationary Schrödinger equation for a number of closed manifolds, all of which share the property that their corresponding quotient spaces can pave the plane without gaps or overlaps. Thanks to this property the motion of a quantum particle on the manifold (and equivalently, on its quotient space) is equivalent to motion in the plane equipped with certain conditions, and enables to express the eigenmode as a superposition of a finite number of plane waves. Moreover, for all the cases discussed the wavefunction experiences perfect revivals after the characteristic revival time T. We have demonstrated reversing of the topological charge of the wave on the Klein bottle at half of the corresponding Talbot time, which is related to its non-orientability. We also showed that time evolution of the wavefunction is equivalent to diffraction on a grating whose complex transmission function satisfies the gluing instructions for the corresponding tessellation of the plane with the copies of the quotient space.

Our work is closely connected with the theory of orbifolds, which in this context are folded surface representations of the smallest repeat unit of a two-dimensional pattern [15]. In particular, all manifolds discussed above are examples of orbifolds, and the gratings with which the quantum motion on these orbifolds can be simulated are elements of 'wallpaper groups'.

The quantum mechanics of particles on compact manifolds, including a sphere, torus, Möbius strip and Klein bottle, have been studied before [14, 25, 26], and an exhaustive account of the periodic functions with the symmetry of each of the wallpaper groups has been given in [27]. Adding to this previous work, here we give the equivalence between the quantum movement of a particle on a compact manifold S and its propagation in the plane equipped with the symmetries of the respective wallpaper group, demonstrating the revival time of the wave on each separate manifold. This equivalence enables a simple simulation of the

propagation using a classical diffraction experiment, from a grating with the symmetry of the appropriate wallpaper group. The diffraction pattern at distance z from the grating is equivalent to the wavefunction of the particle on S at time $t = \mu z/(\hbar k_0)$. In addition, we showed that the topology of the manifold is evident in the number of maxima, minima and saddle points of the wave. Together with the observation of novel phenomena, namely reversing the topological charge on Klein bottle, this can be studied using the proposed optical simulation.

Our method of understanding diffraction also makes contact with several other areas of research. The first is the recent work on so-called glide and twist symmetries [28, 29]. These symmetries are also special cases of the general situation outlined above, where a typical structure is periodic along one axis and has symmetry such that the smallest repeat unit fills the whole space with a combination of translation and inversion operations. One important recent application of this symmetry has been to reduce the dispersion of guided modes [29].

It does not seem to have been previously appreciated that quantum mechanics on folded surfaces can be explored using simple diffraction experiments. Therefore we believe that our method of understanding quantum motion on closed surfaces may represent a new avenue for research, where diffraction from some gratings can be understood in terms of motion of waves on closed surfaces.

Data availability statement

All data that support the findings of this study are included within the article (and any supplementary files).

Acknowledgments

This work was supported by the ESF under the project CZ.02.2.69/0.0/0.0/18_053/0016962. SARH acknowledges financial support from the Royal Society (RPG-2016-186).

Appendix A. Definition and modes of the double-sided square

Double-sided square is a square, on which the wavefunction is defined on both its sides. Although such manifold looks unusual, it is used for Peirce quincuncial projection of a sphere [13]. The quotient space of the double-sided square is a square of side a, with gluing instructions $(a/2 + x, 0) \sim (a/2 - x, 0)$, $(a/2 + x, a) \sim (a/2 - x, a)$, $(0, a/2 + y) \sim (0, a/2 - y)$ and $(a, a/2 + y) \sim (a, a/2 - y)$ (see figure 8(b)). As in the previous cases, a real plane $\mathbb{R}^2$ can be tiled with copies of a function $\psi_0(x, y)$ defined solely on that quotient space. The unit cell of a resulting function $\phi(x, y)$ has a symmetry $\phi(x, y) = \phi(x + a, y + b) = \phi(-x, a - y) = \phi(a - x, -y)$, which leads to the modes $\phi_{mn}(x, y)$

$$\phi_{mn}(x, y) = N_{mn} \cos\left[(m + n)\frac{\pi}{a}x + (m - n)\frac{\pi}{a}\left(y - \frac{a}{2}\right)\right] \tag{A1}$$

with $m, n \in \mathbb{N}_0$ and the normalizing constants $N_{mn} = (1/a)[(1 + \delta_{m0}\delta_{n0})/2]^{-1/2}$. The energy spectrum is $E_{mn} = \pi^2\hbar^2(m^2 + n^2)/(\mu a^2)$ and the revival time is $T = 2\mu a^2/(\pi\hbar)$.

Appendix B. Definition and modes of the double-sided triangle

In this section, we will discuss is a double-sided equilateral triangle of side a. As shown in figure 9(a), the respective quotient space is created by cutting one of the faces from the centre of mass towards the corners of the triangle. When unfolded, this results in a regular hexagon with gluing instructions as these visualised in figure 9(b) (edges labelled with the same colour, e.g. 1 and 1′, are identified). Figure 9(b) shows the plane $\mathbb{R}^2$ tiled with copies of function $\psi_0(x, y)$ defined on σ, using the tessellation rule no. 1. The unit cell of the resulting function $\phi(x, y)$ corresponds to a rectangle with sides $3a$ and $a\sqrt{3}$. This yields the allowed components of the wavevector to be $k_x = 2m\pi/3a$ and $k_y = 2n\pi/a\sqrt{3}$. However, function $\phi(x, y)$ remains unchanged when we move by a vector $(3ma, na\sqrt{3})$ as well as we move along a vector $(3ma + 3a/2, na\sqrt{3} + a\sqrt{3}/2)$. This requires the sum $m + n$ to be equal to an even integer. Finally, the unit cell has a three-fold rotational symmetry and thus the modes $\phi_{mn}(x, y)$ coincide with superpositions of three plane

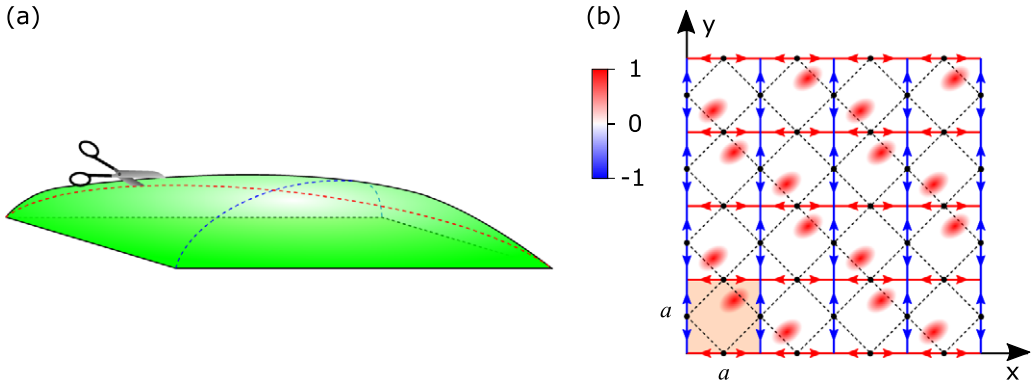

Figure 8. (a) A folded square of a side $a/\sqrt{2}$, where a is a length of its diagonal; (b) The quotient space is equivalent to square of side a, created by cutting the diagonals on one of its sides (e.g., the upper side as indicated in panel (a)). The sides of the original folded square are indicated with black dashed lines and black dots indicate its corners. Panel (b) shows a function $\phi(x, y)$, created by the tessellation with copies of $\psi_0(x, y)$ defined solely on σ.

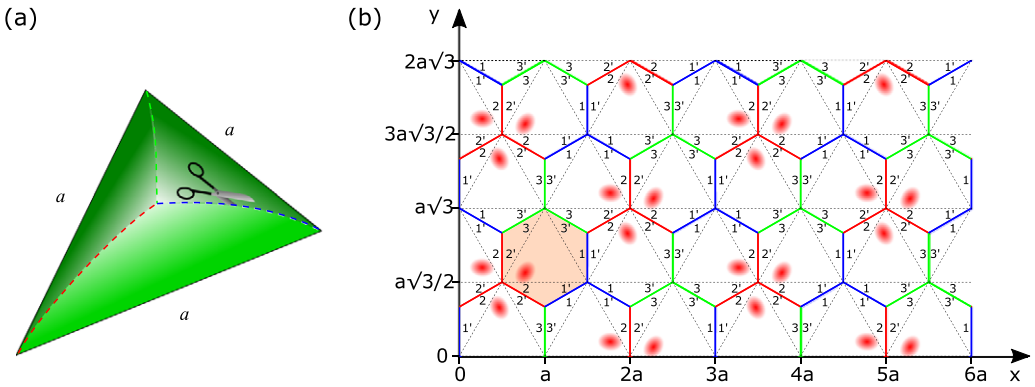

Figure 9. (a) A double-sided regular triangle of a side a. (b) Its quotient space σ, which is a regular hexagon, created by cutting one of the faces of the double-sided triangle from its centre towards the corners and unfolding it. The gluing instructions are visualised with red, green and blue colours (i.e., pairs of edges with the same colour are identified, e.g. the blue edges labelled 1 and 1′). The sides of the original double sided triangle are indicated with black dashed lines. Panel (b) also shows the corresponding tessellation of the plane.

waves with their wavevectors mutually rotated by angle $\pm 2\pi/3$

$$\psi_{mn}(x,y) = N_{mn}\left\{\exp\left[\frac{\mathrm{i}\pi}{a}\left(\frac{2m}{3}x + \frac{2n}{\sqrt{3}}y\right)\right] + \exp\left[\frac{\mathrm{i}\pi}{a}\left(\frac{-m+3n}{3}x - \frac{m+n}{\sqrt{3}}y\right)\right] + \exp\left[\frac{\mathrm{i}\pi}{a}\left(-\frac{m+3n}{3}x + \frac{m-n}{\sqrt{3}}y\right)\right]\right\}, \tag{B1}$$

with normalisation constants $N_{mn} = \left(3\sqrt{3}a^2(1+2\delta_{m0}\delta_{n0})/2\right)^{-\frac{1}{2}}$ and the domain $\mathcal{D}$ for the indices m, n can be expressed as $\mathcal{D} = \{(m,n) = (0,0)\} \cup (\{(m,n); m \in \mathbb{Z}, n \in \mathbb{N}_0, m+n \text{ even}\} \cap \{(m,n); m, n \in \mathbb{Z}, n > -m, m+n \text{ even}\})$. The energy spectrum is $E_{mn} = 2\pi^2\hbar^2(m^2+3n^2)/(9\mu a^2)$ and the revival time is $T = 9\mu a^2/(4\pi\hbar)$.

ORCID iDs

J Bělín https://orcid.org/0000-0002-8801-1606
T Tyc https://orcid.org/0000-0002-7565-6958

References

[1] Szameit A, Dreisow F, Tünnermann S N A, Longhi S, Schultheiss V H, Batz S and Peschel U 2010 Optics in curved space *Phys. Rev. Lett.* **105** 143901

[2] Rinehart R F 1948 A solution of the problem of rapid scanning for radar antennae *J. Appl. Phys.* **19** 860–2
[3] Šarbort M and Tyc T 2012 Spherical media and geodesic lenses in geometrical optics *J. Opt.* **14** 075705
[4] Liao Q, Fonseca N J G and Quevedo-Teruel O 2018 Compact multibeam fully metallic geodesic Luneburg lens antenna based on non-euclidean transformation optics *IEEE Trans. Antennas Propag.* **66** 7383–8
[5] Fonseca N J G, Liao Q and Quevedo-Teruel O 2020 Equivalent planar lens ray-tracing model to design modulated geodesic lenses using non-euclidian transformation optics *IEEE Trans. Antennas Propag.* **68** 3410–22
[6] Pendry J B, Schurig D and Smith D R 2006 Controlling electromagnetic fields *Science* **312** 1780
[7] Leonhardt U and Philbin T G 2006 General relativity in electrical engineering *New J. Phys.* **8** 247
[8] Leonhardt U and Philbin T G 2012 *Geometry and Light: The Science of Invisibility* (New York: Dover)
[9] Leonhardt U and Tyc T 2009 Broadband invisibility by non-euclidean cloaking *Science* **323** 110–2
[10] Jiang W X, Cui T J, Yang X M, Cheng Q, Liu R and Smith D R 2008 Invisibility cloak without singularity *Appl. Phys. Lett.* **93** 194102
[11] Ni X, Wong Z J, Mrejen M, Wang Y and Zhang X 2015 An ultrathin invisibility skin cloak for visible light *Science* **349** 1310–4
[12] Henle M 1979 *A Combinatorial Introduction to Topology* (New York: Dover)
[13] Peirce C S 1879 A quincuncial projection of the sphere *Am. J. Math.* **2** 394–6
[14] Schulte C 1997 Quantum mechanics on the Torus, Klein bottle and projective sphere *Symmetries in Science* vol 9 (Berlin: Springer) pp 313–23
[15] Conway J H, Burgiel H and Goodman-Strauss C 2008 *The Symmetries of Things* (London: Taylor and Francis)
[16] Garcia D G, Chaplain G J, Bělín J, Tyc T, Englert C and Courtial J 2020 Optical triangulations of curved spaces *Optica* **7** 142–7
[17] Bělín J, Horsley S A R and Tyc T 2019 Quantum mechanics and Talbot revivals on a tetrahedron *Phys. Rev.* A **100** 033806
[18] Goodman J W 2005 *Introduction to Fourier Optics* 3rd edn (Englewood, CO: Roberts & Co. Publishers)
[19] Talbot H F 1836 Lxxvi. Facts relating to optical science. no. iv *London Edinburgh Dublin Phil. Mag. J. Sci.* **9** 401–7
[20] Rayleigh. L 1881 Xxv. On copying diffraction-gratings, and on some phenomena connected therewith *London Edinburgh Dublin Phil. Mag. J. Sci.* **11** 196–205
[21] Berry M V and Klein S 1996 Integer, fractional and fractal Talbot effects *J. Mod. Opt.* **43** 2139
[22] Wen J, Zhang Y and Xiao M 2013 The Talbot effect: recent advances in classical optics, nonlinear optics, and quantum optics *Adv. Opt. Photon.* **5** 83–130
[23] Bělín J and Tyc T 2018 Talbot effect for gratings with diagonal symmetry *J. Opt.* **20** 025604
[24] Oprea J 2019 *Differential Geometry and its Applications* vol 59 (Providence, RI: American Mathematical Society)
[25] Hannay J H and Lockwood A 2008 The quantum talbot effect on a sphere *J. Phys. A: Math. Theor.* **41** 395205
[26] Li Z and Ram-Mohan L R 2012 Quantum mechanics on a Möbius ring: energy levels, symmetry, optical transitions, and level splitting in a magnetic field *Phys. Rev.* B **85** 195438
[27] Verberck B 2012 Symmetry-adapted Fourier series for the wallpaper groups *Symmetry* **4** 379–426
[28] Lu L, Fang C, Fu L, Johnson S G, Joannopoulos J D and Soljačić M 2016 Symmetry-protected topological photonic crystal in three dimensions *Nat. Phys.* **12** 337
[29] Dahlberg O, Mitchell-Thomas R C and Quevedo-Teruel O 2017 Reducing the dispersion of periodic structures with twist and polar glide symmetries *Sci. Rep.* **7** 10136